Cerium(IV) Enhances the Catalytic Oxidation Activity of Single-Site Cu Active Sites in MOFs

Xin He,[†] Benjamin G. Looker,[‡] Kimberly T. Dinh,[§] Amanda W. Stubbs,[†] Tian-Yang Chen,[†] Randall J. Meyer,[#] Pedro Serna,[#] Yuriy Román-Leshkov,[§] Kyle M. Lancaster,[‡] Mircea Dincă*,[†]

[†]Department of Chemistry, Massachusetts Institute of Technology, Cambridge, Massachusetts 02139, United States

[‡]Department of Chemistry and Chemical Biology, Cornell University, Baker Laboratory, Ithaca, New York 14853, United States

[§]Department of Chemical Engineering, Massachusetts Institute of Technology, Cambridge, Massachusetts 02139, United States

[#]ExxonMobil Research and Engineering, Annandale, New Jersey 08801, United States

ABSTRACT: The rates of catalytic oxidation of cyclohexane and CO are four and twenty times higher, respectively, with Cu supported on a cerium-based MOF than on the structurally analogous zirconium material. Both Ce- and Zr-based copper catalysts feature uncommon three-coordinate Cu^{II} sites bearing different nuclearities, as determined by Cu K-edge extended X-ray absorption fine structure analysis. These results offer molecular-level understanding of the metal-support interface in MOF catalysts and establish correlations with the more established literature on zirconia and ceria-supported heterogeneous catalysis.

Owing to their molecular-level tunability, metal-organic frameworks (MOFs)[1] are attractive platforms for heterogeneous catalysis. Of particular interest are the inorganic nodes, also known as secondary building units (SBUs), that feature peripheral hydroxo moieties or coordinating water molecules. These provide stable and tunable platforms to support single-site catalysts[2-5] for a range of important reactions,[6-8] such as methane and ethane oxidation,[9-12] CO oxidation,[13] hydrogenations,[14-18] dehydrogenation of light alkanes[19,20] and hydrolysis.[21]

In traditional heterogeneous catalysis, the critical role of the support in regulating the electronic structure of the active site or providing nearby spillover or acid sites, as well as a host of other modulating functions, is well documented.[22-24] By contrast, although studies of catalytic active sites in MOFs are now common, systematic investigations of MOFs as supports are comparatively limited.[25] Given that the acidity[26-28] and electron-withdrawing properties[29,30] of many SBUs are comparable to those of analogous metal oxides,[31] we sought to explore the extent of possible parallels between MOF and ceramic supports by studying the catalytic activity of Cu species in common oxidation reactions when supported on ceria, zirconia, as well as isostructural Ce and Zr-based MOFs.[6,31-33]

Ceria, CeO_2, is particularly intriguing because it enhances the rate of oxidations when used as a support in heterogeneous processes.[23,24,34-42] For instance, the rate of CO oxidation by palladium nanoparticles (NPs) greatly increases when the NPs are supported on ceria, evidenced by a much lower temperature needed to completely oxidize CO. The NPs on ceria reach 100% CO conversion at 90 °C, which is much lower than 170 °C required for the alumina-supported counterpart. It is believed that the interfacial atoms at the corner of the metal NPs exhibit much higher reactivity relative to other perimeter and surface atoms, most likely owing to metal-ceria interactions and low coordination numbers.[23,43,44] Ceria also stabilizes late transition metal single-atom active sites and NPs by preventing sintering, which in turn enhances overall catalytic performance.[36,38] For instance, small Ag NPs supported on ceria show better sinter resistance due to strong binding to the $CeO_2(111)$ face. Inspired by these classic studies in heterogeneous catalysis, we sought to investigate the possibility of observing similar positive enhancements with Ce(IV)-based MOFs and potentially provide an atomic-level understanding of the support-active site interactions responsible for such effects.
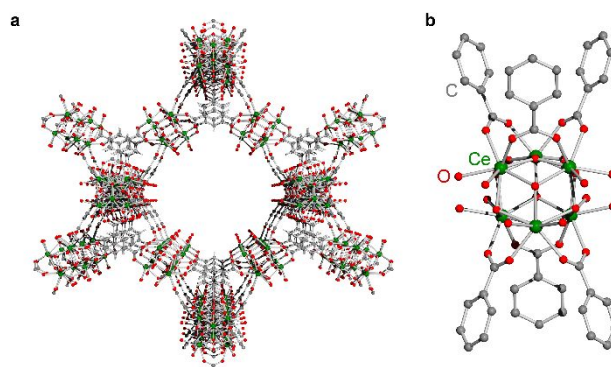

Figure 1. (a) Structure model of MOF-808(Ce) and (b) the Ce$_6$ SBU. Hydrogen atoms are omitted for clarity.
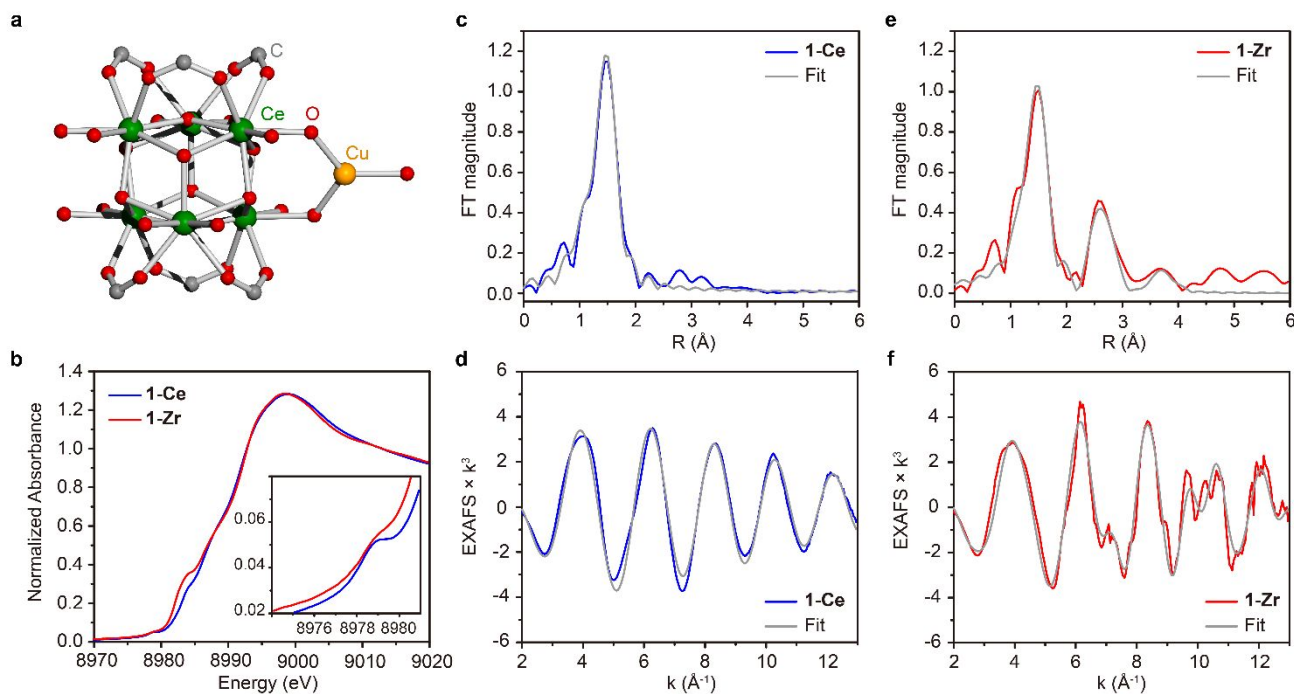
Figure 2. (a) Illustration of the coordination sphere of copper atoms in **1-Ce**. Only one copper atom is showing and hydrogen atoms are omitted for clarity. Color scheme: C, gray; O, red; Ce, green; Cu, yellow. (b) Cu K-edge XANES spectra of **1-Ce** and **1-Zr**. Cu K-edge k^3-weighted EXAFS and Fourier transforms of **1-Ce** (c, d) and **1-Zr** (e, f) overlaid with the best fits.

Hexanuclear Zr_6 carboxylate clusters are some of the most popular SBU supports in MOF catalysis.[7,12,13,45,46] Although isostructural materials with structurally homologous Ce_6 clusters exist, their use in catalysis is decidedly rarer.[25] We surmised that the close structural homology between Zr_6 and Ce_6-based MOFs would allow us to demonstrate the enhancing effect of Ce(IV) and establish functional parallels between MOFs and traditional supports such as ZrO_2 and CeO_2. Herein, we show that, indeed, Cu species supported on isostructural MOF-808(Ce)[47] ($[Ce_6O_4(OH)_{10}(BTC)_2(H_2O)_6]$, BTC^{3-} = benzene-1,3,5-tricarboxylate)[48,49] and MOF-808(Zr) ($[Zr_6O_4(OH)_4(BTC)_2(HCOO)_6]$)[50,51] have differentiated reactivity in the catalytic oxidation of CO and cyclohexane, with the catalyst supported on the Ce MOF exhibiting significantly faster reaction rates. Although electronic effects from Ce(IV) ions are likely at least partially responsible for the observed differences, X-ray absorption experiments surprisingly revealed different nuclearity Cu species on the two MOF supports. These results demonstrate that Zr and Ce-based MOFs induce clear electronic and structural differences in the transition metal catalysts that are supported on their SBUs.

Reactions of $Cu(OAc)_2 \cdot H_2O$ with MOF-808(Ce) and MOF-808(Zr) with in *N,N*-dimethylformamide (DMF) at 100 °C for 24 h yielded $Cu \subset MOF$-808(Ce) (**1-Ce**) and $Cu \subset MOF$-808(Zr) (**1-Zr**) as green microcrystalline solids. The Cu-grafted MOFs retain the same structure and crystallinity as the parent solids, as confirmed by powder X-ray diffraction (PXRD, Figures S1, S2). Compounds **1-Ce** and **1-Zr** also remain porous after copper deposition as verified by N_2 gas sorption experiments (Figure S3, S4), which gave adsorption amounts marginally lower than those of the parent materials, respectively. Thermogravimetric analysis (TGA, Figures S5 and S6) showed significant weight losses for **1-Ce** and **1-Zr** only

above 150 °C and 200 °C, respectively, which were therefore taken as the maximum regeneration temperatures for the two catalysts, respectively.

Initial insight into the nature of the Cu species isolated within **1-Ce** and **1-Zr** came from inductively-coupled plasma mass spectrometry (ICP-MS), which indicated that, on average, 4.0±0.4 and 2.5±0.3 Cu atoms, were clustered on Ce_6 and Zr_6 SBUs, respectively. Cu K-edge X-ray absorption spectroscopy (XAS) measurements provided more precise information about the coordination environment of the Cu atoms. X-ray absorption near edge spectra (XANES), shown in Figure 2b, evidence weak but resolved pre-edge features near 8979 eV, assigned as quadrupole allowed $1s \rightarrow 3d$ excitations. These support the +2 oxidation state for copper species in both MOFs.[10] Furthermore, the MOF architectures lack ligands with low-lying vacant valence orbitals that could participate in quasi-atomic Cu $1s \rightarrow$ "ligand" excitations that would offer the possibility of a Cu^I assignment.

Experimental and simulated Cu-K edge extended X-ray absorption fine structure (EXAFS) data for **1-Ce** and **1-Zr** are shown in Figures 2c and 2d, respectively (see also Supporting Information, Figures S7 and S8 for fitting information about EXAFS of **1-Ce** and **1-Zr**). The EXAFS of **1-Ce** is well-modelled with a single 3-fold degenerate Cu–O path. Improvements made by addition of Cu–Cu and Cu–Ce scattering paths were either negligible or resulted in erroneously large/negative Debye-Waller factors (Table 1). Although a small increase in the quality of the fit can be obtained by fitting two Cu–O–Cu scattering paths, which contributes FT intensity around 3 Å, this addition becomes unreasonable given the model discussed below.

Table 1. EXAFS Simulations for 1-Ce and 1-Zr. [a]

MOF	Fit	Path	CN	R(Å)	±	σ^2	±	F
Cu ⊂ MOF-808(Ce) (**1-Ce**)	1	Cu–O	4	1.926	0.002	0.0065	0.0002	27.90
	2	Cu–O	2	1.927	0.002	0.0019	0.0001	24.40
	3	Cu–O	2	1.924	0.002	0.0026	0.0002	19.28
		Cu–Cu	1	1.934	0.009	0.0200	0.0010	
	4	Cu–O	3	1.925	0.001	0.0040	0.0001	16.26
		Cu–Cu	1	1.741	0.001	0.0391	0.0033	
	5	Cu-O	3	1.926	0.001	0.0042	0.0001	17.03
		Cu–O–Cu	1	3.219	0.014	-0.0011	0.0014	
	6	Cu–O	3	1.926	0.001	0.0042	0.0001	16.98
		Cu–O–Cu	2	3.383	0.015	0.0015	0.0015	
	7	Cu–O	3	1.927	0.001	0.0042	0.0001	17.81
Cu ⊂ MOF-808(Zr) (**1-Zr**)	1	Cu–O	4	1.924	0.004	0.0075	0.0004	50.93
	2	Cu–O	3	1.927	0.004	0.0051	0.0003	47.90
	3	Cu–O	3	1.931	0.003	0.0054	0.0002	38.20
		Cu–Zr	1	2.872	0.005	0.0077	0.0005	
	4	Cu–O	3	1.927	0.002	0.0052	0.0002	30.62
		Cu–Cu	1	3.012	0.004	0.0052	0.0003	
	5	Cu–O	3	1.927	0.002	0.0052	0.0002	28.67
		Cu–Cu	1	3.013	0.003	0.0052	0.0003	
		Cu–Zr	1	4.109	0.010	0.0082	0.0010	

[a]Distance (R) and Debye-Waller factors (σ^2) were allowed to float for different paths, while coordination numbers (CN) were held constant. Goodness of fit is determined by F, defined as $\left[\left(\sum_i^n \left[k_i^3 (EXAFS_{obs} - EXAFS_{calc})_i \right] \right)^2 / n \right]^{1/2}$. Listed errors are fitting errors. Typical errors in CN are ~ 20-25%. Typical distance errors are ± 0.02.

The expected lack of linear Cu–O–Cu bonds should manifest in direct Cu–Cu scattering in the data. Accordingly, without short Cu–Cu distances observed, our XAS results indicated that the copper sites in these constructs are mononuclear Cu^{II} with a coordination sphere completed by three coordinating oxygen atoms (Figure 2a). Notably, CeO_2 itself stabilizes late transition metal atoms and small clusters, which may explain why only mononuclear copper species are present in **1-Ce** even when excess Cu precursor and an elevated temperature are used.[32,38]

In contrast, a non-degenerate Cu–Cu path, and a long, non-degenerate Cu–Zr path are included together with the 3-fold degenerate Cu–O path for fitting the EXAFS data of **1-Zr**. Thus, in **1-Zr**, a copper environment consisting of three oxygen atoms and an additional Cu atom could be readily ascertained. The three-coordinated environments of copper atoms in both **1-Ce** and **1-Zr** are different from reported four-coordinated Cu^{II} species on zirconium MOF NU-1000[10] and highlights the role of the support in determining the coordination environment of the deposited metal species. Three-coordinated Cu^{II} sites have also been observed in UiO-66-supported copper catalyst where each copper(II) ion is coordinated by two oxygen atoms and one chloride anion.[13] Precedent for trigonal-planar Cu(II) ions exists in molecular complex with a 2,4-bis(2,6-diisopropylphenylimido)pentane ligand,[52] as well as in copper-exchanged zeolites.[53]
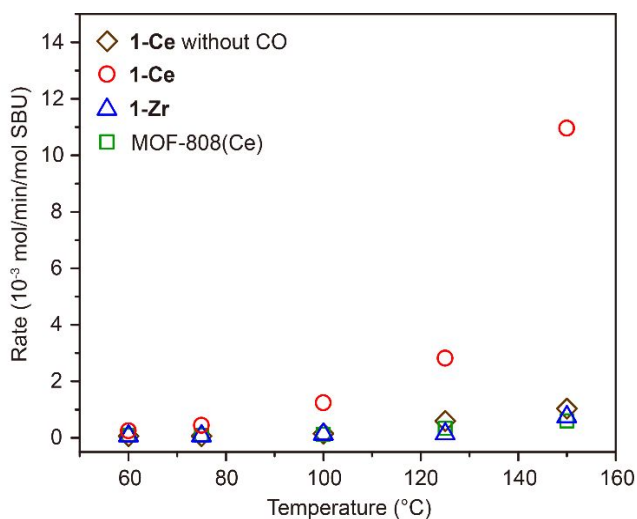

Figure 3. CO oxidation reactivity of MOF-808(Ce) (green square), **1-Ce** (red circle) and **1-Zr** (blue triangle). Reaction rates were measured in 1% CO, 2.5% O_2, 10% N_2, bal He at a flow rate of 1300 mL min^{-1} g$_{cat}^{-1}$ for 25 mg catalyst loading.

With **1-Ce** and **1-Zr** in hand, we sought to investigate the support effect of Ce- and Zr-MOFs and compare it with those observed for

CeO_2 and ZrO_2. A relevant benchmark reaction in this sense is the oxidation of CO, where the Cu/CeO_2 combination is particularly active.[24,37,54,55] Although previous reports showed that Cu-containing MOFs can be active for CO oxidation,[13,56] the impact of the different MOFs as supports has not been addressed. Temperature-programmed reactions were carried out in a tubular reactor loaded with 25 mg of MOF-808(Ce), MOF-808(Zr), **1-Ce**, and **1-Zr**, with a flowing gas feed of 1% CO and 2.5% O_2 in He (see Supporting Information for details). CO oxidation with **1-Zr** and MOF-808(Ce) gave negligible rates at temperatures as high as 125 °C (Figure 3). At 150 °C, the rates for CO_2 production with **1-Zr** and MOF-808(Ce) were 0.74 and 0.59 mmol/min/mol SBU, respectively, indicating that the Cu sites in **1-Zr** are more reactive than ungrafted Ce_6 SBUs. In contrast, **1-Ce** showed significantly increased CO_2 production rates starting as low as 100 °C, exceeding the rates observed for **1-Zr** by a factor of 9, 20, and 14 at 100 °C, 125 °C and 150 °C, respectively. As a control, heating **1-Ce** in a flow of 2.5% O_2 in He in the absence of CO gave only traces of CO_2 at 125 °C, confirming that the CO_2 observed under CO is not produced through framework decomposition.

Previous studies on Cu-Ce catalysts suggested that CO chemisorption is carried out at Cu sites and O_2 activation is promoted by $CuCeO_x$ species involving oxygen vacancies.[57] **1-Ce** bearing both Cu sites and Ce-oxo clusters exhibits significantly higher activity for CO oxidation than **1-Zr** and MOF-808(Ce). Our observation that both Cu and Ce-oxo clusters are required to achieve higher CO oxidation activity is thus in line with what is observed for traditional Cu/CeO_2 catalysts. Most importantly, the CO_2 production rate of **1-Ce** is much higher than that of **1-Zr** between 100 to 150 °C, indicating that MOF-808(Ce) significantly enhances the CO oxidation reactivity of the Cu catalyst. This observation represents a rare example of a Ce^{IV}-MOF enhancing catalytic oxidation reactivity of supported metals, similar to the effect observed in ceria-supported heterogeneous catalysts.[23-25,36,39]
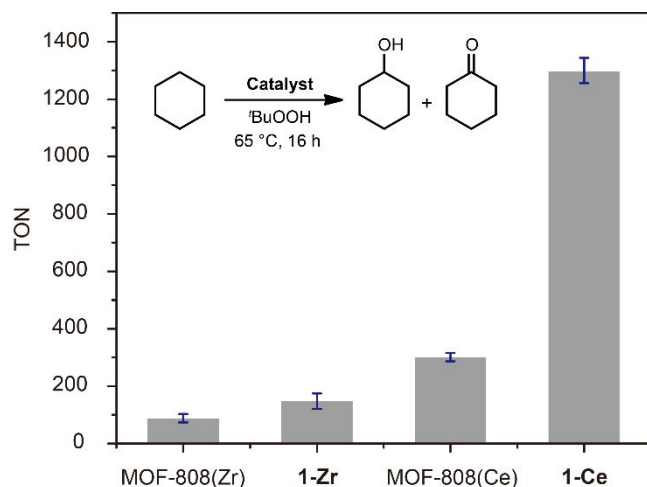

Figure 4. Cyclohexane oxidation with **1-Ce**, **1-Zr**, MOF-808(Ce) and MOF-808(Zr). Reaction conditions: 1 μmol of activated MOF, 1.4 mL 70 wt % ^{t}BuOOH and 4.3 mL cyclohexane for 16 h. TONs were calculated as moles of product generated per mole SBU.

To explore the potential generality of the enhancement provided by the MOF-808(Ce) support versus the Zr analog, we compared the relative catalytic activities of **1-Ce** and **1-Zr** towards cyclohexane oxidation, a liquid-phase reaction. The product of this

transformation, a cyclohexanol/cyclohexanone mixture known as ketone-alcohol (KA) oil, is the main feedstock for intermediates leading to nylon 6 and nylon 66.[58] Cyclohexane oxidation reactions were carried out by heating a suspension of cyclohexane, *tert*-butyl hydroperoxide (^{t}BuOOH) and MOF catalyst at 65 °C for 16 h. Similar to what was observed for CO oxidation, **1-Ce** consistently provided higher turnover numbers (TON) for KA formation than **1-Zr** (Figure 4). We note that radical chain oxidation is widely accepted as the mechanism for cyclohexane oxidation with ^{t}BuOOH to form KA oil.[59,60] The free-radical chains are initiated by metal-assisted decomposition of hydroperoxide to oxygen-centered radicals and are partially terminated in Russell recombination steps. In our case too, the Ce support renders the copper(II) atoms more reducible, likely facilitating peroxide decomposition and generation of oxygen-centered radicals responsible for C–H bond scission and H-atom abstraction from cyclohexane.

The foregoing results establish Ce-based MOFs as superior heterogeneous supports relative to Zr MOFs for oxidation reactions involving Cu-based active catalysts. The results here mimic the trends observed between bulk CeO_2 and ZrO_2. Although we attribute the enhancement observed with the Ce supports to synergistic electronic effects related to distributing the redox burden of the Cu catalyst with the redox-active Ce support, XAS analysis also revealed clear differences in the nature of the Cu species on the two supports: whereas the Ce MOF supports only mononuclear active sites, the Zr support stabilizes higher nuclearity Cu species. Overall, these results highlight the potential utility of MOFs in determining the outcome of heterogeneous catalytic reactions not just as active catalysts, but also as tunable supports, in a strategy inspired by established principles from traditional heterogeneous catalysis.

ASSOCIATED CONTENT

The Supporting Information is available free of charge at ACS Publications website.

Experimental details, PXRD patterns, nitrogen adsorption isotherms, thermogravimetric analysis profiles, and EXAFS simulation residuals (PDF)

AUTHOR INFORMATION

Corresponding Author

*Email: mdinca@mit.edu

Notes

The authors declare no competing financial interests.

ACKNOWLEDGMENT

REFERENCES

(1) Yaghi, O. M.; Kalmutzki, M. J.; Diercks, C. S., *Introduction to Reticular*

Chemistry: Metal–Organic Frameworks and Covalent Organic Frameworks. Wiley-VCH: Weinheim, 2019.

(2) Bakandritsos, A.; Kadam, R. G.; Kumar, P.; Zoppellaro, G.; Medveď, M.; Tuček, J.; Montini, T.; Tomanec, O.; Andrýsková, P.; Drahoš, B.; Varma, R. S.; Otyepka, M.; Gawande, M. B.; Fornasiero, P.; Zbořil, R. Mixed-Valence Single-Atom Catalyst Derived from Functionalized Graphene. *Adv. Mater.* **2019,** *31,* 1900323.

(3) Cui, L.; Cui, L.; Li, Z.; Zhang, J.; Wang, H.; Lu, S.; Xiang, Y. A Copper Single-Atom Catalyst Towards Efficient and Durable Oxygen Reduction for Fuel Cells. *J. Mater. Chem. A* **2019,** 7, 16690-16695.

(4) Yang, H.; Wu, Y.; Li, G.; Lin, Q.; Hu, Q.; Zhang, Q.; Liu, J.; He, C. Scalable Production of Efficient Single-Atom Copper Decorated Carbon Membranes for CO_2 Electroreduction to Methanol. *J. Am. Chem. Soc.* **2019,** *141,* 12717-12723.

(5) Hou, C.-C.; Wang, H.-F.; Li, C.; Xu, Q. From Metal–Organic Frameworks to Single/Dual-Atom and Cluster Metal Catalysts for Energy Applications. *Energy Environ. Sci.* **2020,** 10.1039/C9EE04040D.

(6) Bai, Y.; Dou, Y.; Xie, L.-H.; Rutledge, W.; Li, J.-R.; Zhou, H.-C. Zr-Based Metal-Organic Frameworks: Design, Synthesis, Structure, and Applications. *Chem. Soc. Rev.* **2016,** *45,* 2327-2367.

(7) Islamoglu, T.; Goswami, S.; Li, Z.; Howarth, A. J.; Farha, O. K.; Hupp, J. T. Postsynthetic Tuning of Metal–Organic Frameworks for Targeted Applications. *Acc. Chem. Res.* **2017,** *50,* 805-813.

(8) Drake, T.; Ji, P.; Lin, W. Site Isolation in Metal–Organic Frameworks Enables Novel Transition Metal Catalysis. *Acc. Chem. Res.* **2018,** *51,* 2129-2138.

(9) Xiao, D. J.; Bloch, E. D.; Mason, J. A.; Queen, W. L.; Hudson, M. R.; Planas, N.; Borycz, J.; Dzubak, A. L.; Verma, P.; Lee, K.; Bonino, F.; Crocellà, V.; Yano, J.; Bordiga, S.; Truhlar, D. G.; Gagliardi, L.; Brown, C. M.; Long, J. R. Oxidation of Ethane to Ethanol by N_2O in a Metal–Organic Framework with Coordinatively Unsaturated Iron(II) Sites. *Nat. Chem.* **2014,** *6,* 590-595.

(10) Ikuno, T.; Zheng, J.; Vjunov, A.; Sanchez-Sanchez, M.; Ortuño, M. A.; Pahls, D. R.; Fulton, J. L.; Camaioni, D. M.; Li, Z.; Ray, D.; Mehdi, B. L.; Browning, N. D.; Farha, O. K.; Hupp, J. T.; Cramer, C. J.; Gagliardi, L.; Lercher, J. A. Methane Oxidation to Methanol Catalyzed by Cu-Oxo Clusters Stabilized in NU-1000 Metal–Organic Framework. *J. Am. Chem. Soc.* **2017,** *139,* 10294-10301.

(11) Baek, J.; Rungtaweevoranit, B.; Pei, X.; Park, M.; Fakra, S. C.; Liu, Y.-S.; Matheu, R.; Alshmimri, S. A.; Alshehri, S.; Trickett, C. A.; Somorjai, G. A.; Yaghi, O. M. Bioinspired Metal–Organic Framework Catalysts for Selective Methane Oxidation to Methanol. *J. Am. Chem. Soc.* **2018,** *140,* 18208-18216.

(12) Zheng, J.; Ye, J.; Ortuño, M. A.; Fulton, J. L.; Gutiérrez, O. Y.; Camaioni, D. M.; Motkuri, R. K.; Li, Z.; Webber, T. E.; Mehdi, B. L.; Browning, N. D.; Penn, R. L.; Farha, O. K.; Hupp, J. T.; Truhlar, D. G.; Cramer, C. J.; Lercher, J. A. Selective Methane Oxidation to Methanol on Cu-Oxo Dimers Stabilized by Zirconia Nodes of an NU-1000 Metal–Organic Framework. *J. Am. Chem. Soc.* **2019,** *141,* 9292-9304.

(13) Abdel-Mageed, A. M.; Rungtaweevoranit, B.; Parlinska-Wojtan, M.; Pei, X.; Yaghi, O. M.; Behm, R. J. Highly Active and Stable Single-Atom Cu Catalysts Supported by a Metal–Organic Framework. *J. Am. Chem. Soc.* **2019,** *141,* 5201-5210.

(14) Rungtaweevoranit, B.; Baek, J.; Araujo, J. R.; Archanjo, B. S.; Choi, K. M.; Yaghi, O. M.; Somorjai, G. A. Copper Nanocrystals Encapsulated in Zr-Based Metal–Organic Frameworks for Highly Selective CO_2 Hydrogenation to Methanol. *Nano Lett.* **2016,** *16,* 7645-7649.

(15) An, B.; Zhang, J.; Cheng, K.; Ji, P.; Wang, C.; Lin, W. Confinement of Ultrasmall Cu/ZnO_x Nanoparticles in Metal-Organic Frameworks for Selective Methanol Synthesis from Catalytic Hydrogenation of CO_2. *J. Am. Chem. Soc.* **2017,** *139,* 3834-3840.

(16) Kim, I. S.; Li, Z.; Zheng, J.; Platero-Prats, A. E.; Mavrandonakis, A.; Pellizzeri, S.; Ferrandon, M.; Vjunov, A.; Gallington, L. C.; Webber, T. E.; Vermeulen, N. A.; Penn, R. L.; Getman, R. B.; Cramer, C. J.; Chapman, K. W.; Camaioni, D. M.; Fulton, J. L.; Lercher, J. A.; Farha, O. K.; Hupp, J. T.; Martinson, A. B. F. Sinter-Resistant Platinum Catalyst Supported by Metal-Organic Framework. *Angew. Chem. Int. Ed.* **2018,** *57,* 909-913.

(17) Ji, P.; Song, Y.; Drake, T.; Veroneau, S. S.; Lin, Z.; Pan, X.; Lin, W. Titanium(III)-Oxo Clusters in a Metal–Organic Framework Support Single-Site Co(II)-Hydride Catalysts for Arene Hydrogenation. *J. Am. Chem. Soc.* **2018,** *140,* 433-440.

(18) An, B.; Li, Z.; Song, Y.; Zhang, J.; Zeng, L.; Wang, C.; Lin, W. Cooperative Copper Centres in a Metal–Organic Framework for Selective Conversion of CO_2 to Ethanol. *Nat. Catal.* **2019,** *2,* 709-717.

(19) Li, Z.; Peters, A. W.; Platero-Prats, A. E.; Liu, J.; Kung, C. W.; Noh, H.; DeStefano, M. R.; Schweitzer, N. M.; Chapman, K. W.; Hupp, J. T.; Farha, O. K. Fine-Tuning the Activity of Metal-Organic Framework-Supported Cobalt Catalysts for the Oxidative Dehydrogenation of Propane. *J. Am. Chem. Soc.* **2017,** *139,* 15251-15258.

(20) Li, Z.; Peters, A. W.; Bernales, V.; Ortuño, M. A.; Schweitzer, N. M.; DeStefano, M. R.; Gallington, L. C.; Platero-Prats, A. E.; Chapman, K. W.; Cramer, C. J.; Gagliardi, L.; Hupp, J. T.; Farha, O. K. Metal–Organic Framework Supported Cobalt Catalysts for the Oxidative Dehydrogenation of Propane at Low Temperature. *ACS Cent. Sci.* **2017,** *3,* 31-38.

(21) Mondloch, J. E.; Katz, M. J.; Isley Iii, W. C.; Ghosh, P.; Liao, P.; Bury, W.; Wagner, G. W.; Hall, M. G.; DeCoste, J. B.; Peterson, G. W.; Snurr, R. Q.; Cramer, C. J.; Hupp, J. T.; Farha, O. K. Destruction of Chemical Warfare Agents Using Metal–Organic Frameworks. *Nat. Mater.* **2015,** *14,* 512-516.

(22) Comotti, M.; Li, W.-C.; Spliethoff, B.; Schüth, F. Support Effect in High Activity Gold Catalysts for CO Oxidation. *J. Am. Chem. Soc.* **2006,** *128,* 917-924.

(23) Cargnello, M.; Doan-Nguyen, V. V. T.; Gordon, T. R.; Diaz, R. E.; Stach, E. A.; Gorte, R. J.; Fornasiero, P.; Murray, C. B. Control of Metal Nanocrystal Size Reveals Metal-Support Interface Role for Ceria Catalysts. *Science* **2013,** *341,* 771-773.

(24) Wang, W.-W.; Yu, W.-Z.; Du, P.-P.; Xu, H.; Jin, Z.; Si, R.; Ma, C.; Shi, S.; Jia, C.-J.; Yan, C.-H. Crystal Plane Effect of Ceria on Supported Copper Oxide Cluster Catalyst for Co Oxidation: Importance of Metal–Support Interaction. *ACS Catal.* **2017,** *7,* 1313-1329.

(25) Wang, X.; Zhang, X.; Li, P.; Otake, K.-i.; Cui, Y.; Lyu, J.; Krzyaniak, M. D.; Zhang, Y.; Li, Z.; Liu, J.; Buru, C. T.; Islamoglu, T.; Wasielewski, M. R.; Li, Z.; Farha, O. K. Vanadium Catalyst on Isostructural Transition Metal, Lanthanide, and Actinide Based Metal–Organic Frameworks for Alcohol Oxidation. *J. Am. Chem. Soc.* **2019,** *141,* 8306-8314.

(26) Volkringer, C.; Leclerc, H.; Lavalley, J.-C.; Loiseau, T.; Férey, G.; Daturi, M.; Vimont, A. Infrared Spectroscopy Investigation of the Acid Sites in the Metal–Organic Framework Aluminum Trimesate MIL-100(Al). *J. Phys. Chem. C* **2012,** *116,* 5710-5719.

(27) Driscoll, D. M.; Troya, D.; Usov, P. M.; Maynes, A. J.; Morris, A. J.; Morris, J. R. Characterization of Undercoordinated Zr Defect Sites in UiO-66 with Vibrational Spectroscopy of Adsorbed CO. *J. Phys. Chem. C* **2018,** *122,* 14582-14589.

(28) Zhou, W.; Ma, Z.; Guo, S.; Wang, M.; Wang, J.; Xia, M.; Jia, L.; Hou, B.; Li, D.; Zhao, Y. Comparative Study of CO Adsorption on Zirconia Polymorphs with Drift and Transmission FT-IR Spectroscopy. *Appl. Surf. Sci.* **2018,** *427,* 867-873.

(29) Yang, D.; Odoh, S. O.; Borycz, J.; Wang, T. C.; Farha, O. K.; Hupp, J. T.; Cramer, C. J.; Gagliardi, L.; Gates, B. C. Tuning Zr_6 Metal–Organic Framework (MOF) Nodes as Catalyst Supports: Site Densities and Electron-Donor Properties Influence Molecular Iridium Complexes as Ethylene Conversion Catalysts. *ACS Catal.* **2016,** *6,* 235-247.

(30) Bernales, V.; Yang, D.; Yu, J.; Gumuslu, G.; Cramer, C. J.; Gates, B. C.; Gagliardi, L. Molecular Rhodium Complexes Supported on the Metal-Oxide-Like Nodes of Metal Organic Frameworks and on Zeolite HY: Catalysts for Ethylene Hydrogenation and Dimerization. *ACS Appl. Mater. Interfaces* **2017,** *9,* 33511-33520.

(31) Yang, D.; Gates, B. C. Catalysis by Metal Organic Frameworks: Perspective and Suggestions for Future Research. *ACS Catal.* **2019,** *9,* 1779-1798.

(32) Farmer, J. A.; Campbell, C. T. Ceria Maintains Smaller Metal Catalyst Particles by Strong Metal-Support Bonding. *Science* **2010,** *329,* 933-936.

(33) Haouas, M.; Volkringer, C.; Loiseau, T.; Férey, G.; Taulelle, F. Monitoring the Activation Process of the Giant Pore MIL-100(Al) by Solid State NMR. *J. Phys. Chem. C* **2011,** *115,* 17934-17944.

(34) Esch, F.; Fabris, S.; Zhou, L.; Montini, T.; Africh, C.; Fornasiero, P.; Comelli, G.; Rosei, R. Electron Localization Determines Defect Formation on Ceria Substrates. *Science* **2005,** *309*, 752-755.

(35) Vayssilov, G. N.; Lykhach, Y.; Migani, A.; Staudt, T.; Petrova, G. P.; Tsud, N.; Skála, T.; Bruix, A.; Illas, F.; Prince, K. C.; Matolín, V.; Neyman, K. M.; Libuda, J. Support Nanostructure Boosts Oxygen Transfer to Catalytically Active Platinum Nanoparticles. *Nat. Mater.* **2011,** *10*, 310-315.

(36) Paier, J.; Penschke, C.; Sauer, J. Oxygen Defects and Surface Chemistry of Ceria: Quantum Chemical Studies Compared to Experiment. *Chem. Rev.* **2013,** *113*, 3949-3985.

(37) Elias, J. S.; Risch, M.; Giordano, L.; Mansour, A. N.; Shao-Horn, Y. Structure, Bonding, and Catalytic Activity of Monodisperse, Transition-Metal-Substituted CeO_2 Nanoparticles. *J. Am. Chem. Soc.* **2014,** *136*, 17193-17200.

(38) Jones, J.; Xiong, H.; DeLaRiva, A. T.; Peterson, E. J.; Pham, H.; Challa, S. R.; Qi, G.; Oh, S.; Wiebenga, M. H.; Pereira Hernández, X. I.; Wang, Y.; Datye, A. K. Thermally Stable Single-Atom Platinum-on-Ceria Catalysts Via Atom Trapping. *Science* **2016,** *353*, 150-154.

(39) Montini, T.; Melchionna, M.; Monai, M.; Fornasiero, P. Fundamentals and Catalytic Applications of CeO_2-Based Materials. *Chem. Rev.* **2016,** *116*, 5987-6041.

(40) Zuo, Z.; Ramírez, P. J.; Senanayake, S. D.; Liu, P.; Rodriguez, J. A. Low-Temperature Conversion of Methane to Methanol on CeO_x/Cu_2O Catalysts: Water Controlled Activation of the C–H Bond. *J. Am. Chem. Soc.* **2016,** *138*, 13810-13813.

(41) Danielis, M.; Colussi, S.; de Leitenburg, C.; Soler, L.; Llorca, J.; Trovarelli, A. Outstanding Methane Oxidation Performance of Palladium-Embedded Ceria Catalysts Prepared by a One-Step Dry Ball-Milling Method. *Angew. Chem. Int. Ed.* **2018,** *57*, 10212-10216.

(42) Lustemberg, P. G.; Palomino, R. M.; Gutiérrez, R. A.; Grinter, D. C.; Vorokhta, M.; Liu, Z.; Ramírez, P. J.; Matolín, V.; Ganduglia-Pirovano, M. V.; Senanayake, S. D.; Rodriguez, J. A. Direct Conversion of Methane to Methanol on Ni-Ceria Surfaces: Metal–Support Interactions and Water-Enabled Catalytic Conversion by Site Blocking. *J. Am. Chem. Soc.* **2018,** *140*, 7681-7687.

(43) Williams, W. D.; Shekhar, M.; Lee, W. S.; Kispersky, V.; Delgass, W. N.; Ribeiro, F. H.; Kim, S. M.; Stach, E. A.; Miller, J. T.; Allard, L. F. Metallic Corner Atoms in Gold Clusters Supported on Rutile Are the Dominant Active Site During Water-Gas Shift Catalysis. *J. Am. Chem. Soc.* **2010,** *132*, 14018-14020.

(44) Shekhar, M.; Wang, J.; Lee, W. S.; Williams, W. D.; Kim, S. M.; Stach, E. A.; Miller, J. T.; Delgass, W. N.; Ribeiro, F. H. Size and Support Effects for the Water-Gas Shift Catalysis over Gold Nanoparticles Supported on Model Al_2O_3 and TiO_2. *J. Am. Chem. Soc.* **2012,** *134*, 4700-4708.

(45) Desai, S. P.; Ye, J.; Zheng, J.; Ferrandon, M. S.; Webber, T. E.; Platero-Prats, A. E.; Duan, J.; Garcia-Holley, P.; Camaioni, D. M.; Chapman, K. W.; Delferro, M.; Farha, O. K.; Fulton, J. L.; Gagliardi, L.; Lercher, J. A.; Penn, R. L.; Stein, A.; Lu, C. C. Well-Defined Rhodium–Gallium Catalytic Sites in a Metal–Organic Framework: Promoter-Controlled Selectivity in Alkyne Semihydrogenation to E-Alkenes. *J. Am. Chem. Soc.* **2018,** *140*, 15309-15318.

(46) Liu, J.; Ye, J.; Li, Z.; Otake, K.-i.; Liao, Y.; Peters, A. W.; Noh, H.; Truhlar, D. G.; Gagliardi, L.; Cramer, C. J.; Farha, O. K.; Hupp, J. T. Beyond the Active Site: Tuning the Activity and Selectivity of a Metal–Organic Framework-Supported Ni Catalyst for Ethylene Dimerization. *J. Am. Chem. Soc.* **2018,** *140*, 11174-11178.

(47) The material was first reported as Ce-BTC and is denoted here as MOF-808-(Ce) for consistency with the Zr analogue MOF-808-(Zr).

(48) Lammert, M.; Glißmann, C.; Reinsch, H.; Stock, N. Synthesis and Characterization of New Ce(IV)-MOFs Exhibiting Various Framework Topologies. *Cryst. Growth Des.* **2017,** *17*, 1125-1131.

(49) Ji, P.; Sawano, T.; Lin, Z.; Urban, A.; Boures, D.; Lin, W. Cerium-Hydride Secondary Building Units in a Porous Metal–Organic Framework for Catalytic Hydroboration and Hydrophosphination. *J. Am. Chem. Soc.* **2016,** *138*, 14860-14863.

(50) Furukawa, H.; Gándara, F.; Zhang, Y.-B.; Jiang, J.; Queen, W. L.; Hudson, M. R.; Yaghi, O. M. Water Adsorption in Porous Metal–Organic Frameworks and Related Materials. *J. Am. Chem. Soc.* **2014,** *136*, 4369-4381.

(51) Jiang, J.; Gándara, F.; Zhang, Y.-B.; Na, K.; Yaghi, O. M.; Klemperer, W. G. Superacidity in Sulfated Metal–Organic Framework-808. *J. Am. Chem. Soc.* **2014,** *136*, 12844-12847.

(52) Holland, P. L.; Tolman, W. B. Three-Coordinate Cu(II) Complexes: Structural Models of Trigonal-Planar Type 1 Copper Protein Active Sites. *J. Am. Chem. Soc.* **1999,** *121*, 7270-7271.

(53) Dinh, K. T.; Sullivan, M. M.; Narsimhan, K.; Serna, P.; Meyer, R. J.; Dincă, M.; Roman-Leshkov, Y. Continuous Partial Oxidation of Methane to Methanol Catalyzed by Diffusion-Paired Copper Dimers in Copper-Exchanged Zeolites. *J. Am. Chem. Soc.* **2019,** *141*, 11641-11650.

(54) Freund, H. J.; Meijer, G.; Scheffler, M.; Schlogl, R.; Wolf, M. Co Oxidation as a Prototypical Reaction for Heterogeneous Processes. *Angew. Chem. Int. Ed.* **2011,** *50*, 10064-10094.

(55) Wang, F.; Büchel, R.; Savitsky, A.; Zalibera, M.; Widmann, D.; Pratsinis, S. E.; Lubitz, W.; Schüth, F. In Situ EPR Study of the Redox Properties of $CuO–CeO_2$ Catalysts for Preferential CO Oxidation (PROX). *ACS Catal.* **2016,** *6*, 3520-3530.

(56) Tu, B.; Pang, Q.; Xu, H.; Li, X.; Wang, Y.; Ma, Z.; Weng, L.; Li, Q. Reversible Redox Activity in Multicomponent Metal–Organic Frameworks Constructed from Trinuclear Copper Pyrazolate Building Blocks. *J. Am. Chem. Soc.* **2017,** *139*, 7998-8007.

(57) Jia, A.-P.; Hu, G.-S.; Meng, L.; Xie, Y.-L.; Lu, J.-Q.; Luo, M.-F. CO Oxidation over $CuO/Ce_{1-x}Cu_xO_{2-\delta}$ and $Ce_{1-x}Cu_xO_{2-\delta}$ Catalysts: Synergetic Effects and Kinetic Study. *J. Catal.* **2012,** *289*, 199-209.

(58) Musser, M. T. Cyclohexanol and Cyclohexanone. In *Ullmann's Encyclopedia of Industrial Chemistry*, Wiley-VCH: Weinheim, 2012; Vol. 11, pp 49-58.

(59) Nowotny, M.; Pedersen, L. N.; Hanefeld, U.; Maschmeyer, T. Increasing the Ketone Selectivity of the Cobalt-Catalyzed Radical Chain Oxidation of Cyclohexane. *Chem. Eur. J.* **2002,** *8*, 3724-3731.

(60) Martins, L.; Nasani, R.; Saha, M.; Mobin, S.; Mukhopadhyay, S.; Pombeiro, A. Greener Selective Cycloalkane Oxidations with Hydrogen Peroxide Catalyzed by Copper-5-(4-Pyridyl)Tetrazolate Metal-Organic Frameworks. *Molecules* **2015,** *20*, 19203-19220.

1
2
3
4
5
6
7
8
9
10
11
12
13
14
15
16
17
18
19
20
21
22
23
24
25
26
27
28
29
30
31
32
33
34
35
36
37
38
39
40
41
42
43
44
45
46
47
48
49
50
51
52
53
54
55
56
57
58
59
60

Table of Contents artwork

Reactivity Enhancement of Copper Catalyst

CO O$_2$

^{t}BuOOH

OH

CO$_2$

by a Cerium(IV) Metal–Organic Framework